



# On thermal runaway and local endothermic/exothermic reactions during flash sintering of ceramic nanoparticles

Rachman Chaim, Claude Estournès

## ► To cite this version:

Rachman Chaim, Claude Estournès. On thermal runaway and local endothermic/exothermic reactions during flash sintering of ceramic nanoparticles. *Journal of Materials Science*, 2018, vol. 53 (n° 9), pp. 6378-6389. 10.1007/s10853-018-2040-y . hal-01744259

**HAL Id: hal-01744259**

**<https://hal.science/hal-01744259>**

Submitted on 27 Mar 2018

**HAL** is a multi-disciplinary open access archive for the deposit and dissemination of scientific research documents, whether they are published or not. The documents may come from teaching and research institutions in France or abroad, or from public or private research centers.

L'archive ouverte pluridisciplinaire **HAL**, est destinée au dépôt et à la diffusion de documents scientifiques de niveau recherche, publiés ou non, émanant des établissements d'enseignement et de recherche français ou étrangers, des laboratoires publics ou privés.




## Open Archive TOULOUSE Archive Ouverte (OATAO)

OATAO is an open access repository that collects the work of some Toulouse researchers and makes it freely available over the web where possible.

This is an author's version published in : <http://oatao.univ-toulouse.fr/19655>

**Official URL :** <https://dx.doi.org/10.1007/s10853-018-2040-y>

### **To cite this version :**

Chaim, Rachman and Estournès, Claude  *On thermal runaway and local endothermic/exothermic reactions during flash sintering of ceramic nanoparticles.* (2018) Journal of Materials Science, vol. 53 (n° 9). pp. 6378-6389. ISSN 0022-2461

Any correspondence concerning this service should be sent to the repository administrator :  
[tech-oatao@listes-diff.inp-toulouse.fr](mailto:tech-oatao@listes-diff.inp-toulouse.fr)

# On thermal runaway and local endothermic/exothermic reactions during flash sintering of ceramic nanoparticles

Rachman Chaim<sup>1,\*</sup>  and Claude Estournès<sup>2</sup>

<sup>1</sup>Department of Materials Science and Engineering, Technion – Israel Institute of Technology, 32000 Haifa, Israel

<sup>2</sup>Université de Toulouse, CIRIMAT, CNRS INPT UPS, Université Paul-Sabatier, 118 route de Narbonne, 31062 Toulouse Cedex 9, France

## ABSTRACT

Numerical analysis of the heat balance at the flash event during flash sintering of granular ceramic nanoparticles was performed assuming continuum solid state as well as simultaneous surface softening/liquid formation and current percolation through the nanoparticle contacts. Assuming inter-particle radiations in the specimen volume, the electric Joule heat generated at the nanoparticle contacts partially lost by radiation from the specimen external surfaces. Considering the thermal effects due to rapid heating rate and free-molecular heat conduction regime, high-temperature gradients between the nanoparticle surfaces and the surrounding gas were developed. The attractive capillary forces, induced by the particle surface softening/liquid at the percolation threshold, lead to rapid rearrangement and densification of the nanoparticles. The excess Joule heat, already at the flash event, suffices the excess internal heat that is necessary for partial or full melting. Particle surface softening/liquid formation is a transient process, hence followed by crystallization immediate after the nanoparticle rearrangement. Thermal runaway is associated with local surface softening/melting and its solidification.

## Introduction

Flash sintering (FS) is a novel technique, whereby simultaneous application of electric and thermal fields lead, within few seconds, to ultrafast densification of the ceramic nanoparticles compact [1, 2]. The sudden densification takes place at appropriate combinations of the electric field and temperature

and accompanied by the photoluminescence flash [3]. The photoemission during the flash was related to different sources, such as electroluminescence due to electron-hole recombination [3–5], dielectric breakdown [6], and as incandescence emission [7]. The photoluminescence signals the transition to the non-linear behavior of the compact's electric conductivity, which otherwise is almost linear with the increase in

the temperature [8, 9]. Immediately after the flash event, the initial voltage control mode (i.e., constant voltage) exchanged into the current control mode (i.e., constant current) in order to prevent damage of the specimen and the flash sintering system [10, 11].

The so-called incubation-time is the time between the electric field application, at constant temperature, and the flash event. The dissipated power density acquired during this period is a few tens of  $\text{W cm}^{-3}$ , irrespective of the ceramic composition [12]. In this respect, heat balance calculations were consistent with the formation of plasma at the nanoparticle contacts [13]. Although the thermal runaway of the Joule heating is a well-accepted description of the process physics [14–16], the underlying atomistic mechanisms for the rapid sintering are still under debate. The main question is whether the enhanced mass transport takes place at the nanoparticle surfaces [17–20], or within their bulk [21], in the solid state [21, 22], or liquid-assisted [23–26].

Different densification mechanisms were proposed for FS especially due to the serious uncertainty in measuring the actual temperatures within the specimen [27–29]. Macroscopic temperature gradients between tens of degrees [30, 31] and several thousand degrees [13, 14, 32] were estimated between the gauge length and the electrodes. However, local temperature gradients of up to 300 °C were estimated between the particle centers and the grain boundary at their connecting necks [33]. Recent percolation model showed the possibility for nanoparticle surface softening/melting at temperatures resembling plasma and in excess of the melting points [13]. This was in agreement with observed dielectric pre-breakdown in alumina [10, 34]. In addition, several teams challenged recently the electric field effects in flash sintering, by conducting high heating rate sintering experiments in the absence of the electric field. Ji et al. [22] applied high heating rates without electric field, in addition to conventional, SHS (self-propagating high-temperature synthesis), and flash sintering, for comparative sintering studies in yttria-stabilized zirconia (3YSZ). Sudden insertion of the specimens into the furnace hot zone enabled fast heating rate of  $\sim 50\text{ }^{\circ}\text{C s}^{-1}$ . Dense specimens formed by the latter technique after a few minutes were comparable to the flash sintered specimens. The authors concluded that the rapid heating is partially responsible for the rapid densification during the flash sintering. These observations support the

significant role of the thermal effects and gradients, which otherwise were underestimated during the flash sintering. The lack of liquid residue in many flash sintered microstructures may be due to the limited extent of the softened/melted surface (i.e., a few atomic layers at the particle surfaces) as well as due to its metastable and transient nature. Nevertheless, when formation of high-temperature liquid led to selective evaporation of some elements, liquid-like phases were observed at the particle surfaces and grain boundaries [35, 36]. Nevertheless, local melting was observed at the pore surfaces during flash spark plasma sintering (FSPS) of thermoelectric Sb-doped magnesium-tin silicide [37].

In the present paper, we analyze the thermal processes involved in flash sintering of ceramic nanoparticles and perform the heat balance at the flash event to evaluate the conditions needed for the flash. We will show that the formation of liquid at the particle contacts, i.e., surface softening, is an immediate and transient process. The ultrafast densification is due to the particle rearrangement enhanced by the attractive capillary forces due to the liquid. Therefore, the so-called thermal runaway is associated with the local endothermic softening/melting at the nanoparticle surfaces and its exothermic solidification.

## Theory

### Heat transfer from nanoparticles

Our basic assumption is that the granular nanoparticle system subjected to heat and electric field can be visualized as a network of resistors, which represent the particles (i.e., low bulk resistivity) and their contacts (high interfacial resistivity); the latter are preferable for local Joule heating. Due to the isolating nature of the ceramics, the electric current will flow through the path with minimum local and overall electric resistance in this network. Nevertheless, the contacts with the highest electric resistance along this path will be the ones who will preferably be heated to reach the local melting. Lebrun et al. [30] estimated the thermal relaxation time, i.e., the time needed for thermal equilibration across the nanoparticle. Using their approach and the typical density and thermal properties of 3 mol% yttria-stabilized zirconia (3YSZ) above the Debye temperature (540 K), relaxation

times of 50 ns and 20  $\mu$ s may be calculated for nanoparticles with radii of 50 and 1000 nm, respectively. These durations are shorter by nine and six orders of magnitude, respectively, compared to the flash event duration of 1 s. At first glance, this analysis shows that at regular steady-state conditions, thermal equilibration is an immediate process, and the heat generated at the nanoparticle contact transferred to the nanoparticle center, to raise the nanoparticle temperature as a whole. However, the specimens in flash sintering often hanged by two electrodes, which in turn do not visually exhibit an increase in their temperature within the furnace. Therefore, heat loss by conduction from the specimen is negligible. Furthermore, heat transfer by conduction/convection from the hot nanoparticle surface to its surrounding gas may follow different regimes, depending on the nanoparticle size and the gas composition, as will be shown below. In addition, changing the heating rate led to different sintering rates in both the presence and absence of the electric field [22, 38]. Consequently, the heating rate has strong effect on the heat transfer regime and mechanism during sintering hence heat transfer needs careful treatment.

### Conduction heat transfer

For the nanoparticle subjected to sudden temperature increase, the heat transfer regime depends on the Knudsen number, which is the ratio between the mean free path ( $\lambda_{\text{MFP}}$ ) of the surrounding gas molecules (at the given gas temperature and pressure conditions), and the characteristic length scale of the nanoparticle, i.e., the nanoparticle radius,  $r$  [39]:

$$Kn = \frac{\lambda_{\text{MFP}}}{r} \quad (1)$$

Liu et al. [39] thoroughly reviewed the regimes of conduction heat transfer from hot nanoparticles. In this respect, thermal conduction from hot nanoparticles to the surrounding gas takes place by free-molecular (FM) regime in contrast to the continuum regime, which is applicable for the hot conventional-size particles. For  $Kn \leq 0.01$  heat transfer is regarded as in continuum heat transfer regime, where the heat transfer rate is expressed by:

$$\dot{Q}_{\text{cond}}^{\text{continuum}} = 4\pi r k_g^* (T_p - T_{\text{furn}}) \quad (2)$$

where  $T_p$  and  $T_{\text{furn}}$  are the nanoparticle and the furnace (gas) temperatures, respectively, and  $k_g^*$  is the temperature-dependent thermal conduction coefficient of the gas.

However, for  $Kn \geq 1.0$  the free-molecular regime dominates, according to [39]:

$$\dot{Q}_{\text{cond}}^{\text{FM}} = 4\pi r^2 \left( \frac{\alpha}{2 - \alpha} \right) \frac{p_g (c_{p,g} - \frac{R}{2})}{\sqrt{2\pi R T_g}} (T_p - T_{\text{furn}}) \quad (3)$$

where  $p_g$  is the gas pressure,  $c_{p,g}$  is the specific heat of gas at constant pressure,  $R$  is the gas constant, and  $\alpha$  is the thermal accommodation coefficient of the nanoparticle material in the surrounding gas.

For intermediate  $Kn$  values, a transition regime exists, which is expressed by various interpolation methods of the continuum and the free-molecular regimes. Typical values of the mean free path for the air molecules are 68 and 500 nm at 273 and 1500 K, respectively [39]. Thus, nanoparticles smaller than 1  $\mu$ m in diameter, rapidly heated to 1500 K, will lose heat by free-molecular regime, i.e., hardly lose heat, hence will develop high-temperature gradient at their surface (Knudsen layer), with respect to their surrounding gas. This is in agreement with the measured specimens' surface temperatures, which are far higher than the actual furnace temperature during the flash sintering [29, 40].

The above treatment has two implications. First, that heat loss, from suddenly heated nanoparticles, by conduction/convection into the gas is negligibly small at high temperatures, as is typical for ceramic nanoparticles subjected to flash sintering. Second, and more important, is that at the nano-scale particle size range, in green compacts with low green density, the free-molecular heat transfer regime imposes Knudsen layer at the nanoparticle surfaces, with temperatures higher than their surrounding gas temperature. Therefore, in addition to negligible heat loss by conduction/convection from the surface, the sudden increase in the Joule heating at the nanoparticle contacts increases, in turn, the temperature gradient between the nanoparticle surface and the surrounding gas. The temperature in this layer may increase as high as twice the surrounding gas temperature, if the nanoparticles are rapidly heated [41, 42]. Therefore, this subsection is to emphasize the possible formation of high-temperature gradients at the nanoparticle surfaces due to the heat transfer regime, and we neglect the conducted heat.

High-temperature gradients were measured between the specimen surface and the furnace temperature in 8-YSZ system [29], ZnO [43], and SiC [44]. Grasso et al. [27] used finite element model to calculate the temperature distribution during flash sintering of 3-YSZ. Using the specimen data and surface flash sintering temperature of 850 °C measured by Cologna et al. [1], they calculated temperatures in excess of 1600 °C that developed within 3 s at 120 V cm<sup>-1</sup> for power of 70 W. The temperatures derived from their simulation were always higher than those calculated assuming black-body radiation of dense specimen [21]. However, these temperature gradients are still too low for fulfilling the demand for ultrafast densification kinetics by solid-state sintering. Therefore, the question about the actual sink of the Joule heat at the contact points becomes very important and crucial for understanding the flash process mechanism and kinetics.

### Radiation heat transfer

First, it is worth noting that ultrafine powder beds exhibit thermal conductivities lower by orders of magnitude compared to their dense solid counterparts, especially at high temperatures [45]. At high temperatures, radiation is the most effective heat transfer mechanism in dense ceramics, due to its strong temperature dependence. However, the effective thermal insulating ability of the ultrafine powder arises from refraction, reflection, and absorption of the radiated heat at the nanoparticle surfaces; thus, the heat is absorbed by the nanoparticles instead of its transfer across the powder bed. Similar effects may be applicable to fine ceramic nanoparticles subjected to rapid heating. Therefore, we will pay a special attention to the total radiated heat and its portion that may be absorbed within the nanoparticles and raise their temperature.

Let us assume a homogeneous ceramic compact of spherical nanoparticles with radius  $r$ , green density  $\rho$  (%), and theoretical density  $\rho_o$ , subjected to flash sintering. It has acquired thermal heat according to its heat capacity, by absorbing heat from the furnace (up to  $T_{\text{furn}}$ ). Increasing the current at constant voltage at this temperature leads to Joule heating. This heat, which preferably generated at the particle contacts, immediately absorbed by the nanoparticle, to heat up its volume and to increase its temperature. This heat generation and transfer should take place at

all nanoparticles with contacts. However, this Joule heat, which pumped from the contacts into the nanoparticle, should be radiated out, due to the higher temperature of the nanoparticles relative to their surrounding gas temperature. Assuming homogeneous distribution of the nanoparticles *inside* the specimen, the average radiated heat from each nanoparticle to its neighbors is equal to the radiated heat that this nanoparticle gains from its neighbors. Therefore, the internal particles practically do not lose heat. The Joule heat generated at the nanoparticle contacts is preserved at each nanoparticle, increasing its surface temperature at the flash event to  $T_p$ . The radiated heat loss is only from the particles constituting the external surface of the powder compact, which lack neighbors. Following these assumptions, the heat radiated from a single nanoparticle  $\dot{q}_{\text{rad}}^p$  to its surrounding gas is [18]:

$$\dot{q}_{\text{rad}}^p = 4\pi r^2 \cdot \varepsilon_{\text{em}} \sigma_{\text{SB}} (T_p^4 - T_{\text{furn}}^4) \quad (4)$$

where  $\varepsilon_{\text{em}}$  is the nanoparticles' emissivity,  $\sigma_{\text{SB}}$  is the Stefan–Boltzmann constant for black-body radiation, and  $T_p$  and  $T_{\text{furn}}$  are the temperatures at the nanoparticle surface, and of the furnace (gas) surrounding the nanoparticle, respectively.

The number of the nanoparticles at the external radiating surfaces of the specimen,  $N_s$ , is the total external surfaces divided by the surface of the hemispherical particle:

$$N_s = \frac{\rho \cdot A_s}{2\pi r^2} \quad (5)$$

where  $A_s$  is the thermal radiating surface of the specimen, and the factor 2 in the denominator is a geometric correction factor due to the microscopic hemispherical surface of the particle in comparison with the macroscopic planar surface of the specimen.

Since the radiated heat in Eq. (4) inter-radiated between the internal nanoparticles, which surrounded by other nanoparticles, we assume that it is absorbed by the neighboring nanoparticles. Thus, the only radiated heat that is lost to the gas/furnace is from the nanoparticles at the external surfaces of the specimen (surfaces facing the furnace walls). We calculate this radiated heat  $\dot{Q}_{\text{rad}}^{\text{surf}}$  by multiplying Eqs. (4) and (5) as:

$$\dot{Q}_{\text{rad}}^{\text{surf}} = \rho \cdot A_s \cdot \varepsilon_{\text{em}} \sigma_{\text{SB}} (T_{\text{surf}}^4 - T_{\text{furn}}^4) \quad (6)$$

The nanoparticles in Eq. (6) are characterized by the specimen surface temperature,  $T_{\text{surf}}$  as often



measured by a pyrometer, that is lower from  $T_p$ , the nanoparticle surface temperature inside the specimen [Eq. (4)]. Therefore, we consider the radiation term in Eq. (6) as the only radiated heat lost from the specimen, whereas the other portions of the radiated heat are stored within the specimen. Equation (6) with omitted  $\rho$  is often used for the heat balance during the flash sintering, when assuming the specimen as a solid continuum.

### Heat balance at flash event

We showed above that heat loss by convection/conduction is negligible in flash sintering. Moreover, only part of the Joule heat that generated at the nanoparticle contacts is lost by radiation from the specimen external surfaces. The rest of the electric heat is spent to increase the particle's surface temperature via inter-radiation between the nanoparticles in the bulk of the specimen. Therefore, the next step is to set the heat balance via the rate equation at the flash event, in order to determine possible melting at the nanoparticle contacts. We restrict our treatment below to local liquid formation/particle surface softening due to Joule heating and neglect the plasma effects that may form at the gaps between the nanoparticles. Moreover, the oxidation/reduction processes at the electrodes were neglected as they are local and their contribution to the overall electric resistance of the system was reported as negligible [46]. The rate equation that describes the heat balance is [18, 47]:

$$\dot{Q}_{\text{int}} = \dot{Q}_{\text{Joul}} - \dot{Q}_{\text{rad}} - \dot{Q}_{\text{cond}} \quad (7)$$

where  $\dot{Q}_{\text{int}}$  is the internal heat, accumulated in the specimen,  $\dot{Q}_{\text{Joul}}$  is the Joule heat input,  $\dot{Q}_{\text{rad}}$  and  $\dot{Q}_{\text{cond}}$  are the heats lost by radiation and conduction, respectively.

Based on our treatment above, we neglect the conducted heat term. Using the modified equations for the radiated heat in the heat balance equation, one receives for flash sintering:

$$\rho \rho_o c_p \frac{dT}{dt} = \frac{L_s}{A_{cs}} \frac{V^2}{R_e} - \rho \cdot \frac{A_s}{V_s} \cdot \varepsilon_{\text{em}} \sigma_{\text{SB}} (T_{\text{surf}}^4 - T_{\text{furn}}^4) \quad (8)$$

where  $\rho$  is the green density,  $\rho_o$  is the theoretical density,  $c_p$  is the specific heat capacity,  $V$  is the applied electric field per unit length (dog-bone specimens),  $R_e$  is the specimens' electric resistance,

$V_s$ ,  $L_s$ , and  $A_{cs}$  are the specimen volume, length, and cross-section area, respectively.

The parameters  $c_p$  and  $R_e$  in Eq. (8) are temperature-dependent, and integration was performed while taking into account their temperature dependencies (see "Appendix" section).

### Calculations and results

We selected the material and flash sintering parameters from the literature, whenever detailed data were available. The following data from Cologna et al. [2] for flash sintered Mg-doped alumina (0.25 wt% MgO) specimens were used. Dog-bone specimens heated to 1400 °C at the 10 °C min<sup>-1</sup> heating rate, under DC electric field of  $V = 1000 \text{ V cm}^{-1}$ , with  $A_s = 2.04 \text{ cm}^2$ ,  $V_s = 0.1188 \text{ cm}^3$ ,  $\rho = 0.55 \pm 0.01$ ,  $\rho_o = 3.99 \text{ g cm}^{-3}$ , and average particle radius  $r = 100 \text{ nm}$ . The various aspects of the calculations and the material properties presented and explained in the "Appendix" section.

We assumed formation of softening/liquid at the nanoparticle contacts for the current percolation. Nevertheless, we also used the reported temperature-dependent conductivity of the specimen in the solid state with no liquid effects [2]. This choice also enables fair comparison of the present results to those published in the literature, when assuming solid-state sintering. The methodology of the present calculations is as follows:

First, we used the rate Eq. (7) to determine the flash onset temperature, as was performed by Raj [21], Zhang and Luo [43], and others. In this approach, the flash temperature is defined when the rate of Joule heat formation surpasses the heat dissipation rate by radiation. In this respect, the derivative of the two terms  $\dot{Q}_{\text{Joul}}$  and  $\dot{Q}_{\text{rad}}$  at the right-hand side of Eq. (7) are plotted versus temperature; the intersection between the two curves, where the rate of Joule heat formation becomes higher than the rate of heat dissipation, defines the flash temperature. The calculated flash temperatures using equation (S3) in Zhang and Luo [43], and our present approach, resulted in 1260 and 1220 °C, respectively, as shown in Fig. 1. Cologna et al. [2] reported the flash temperature of  $\sim 1260 \text{ °C}$  at  $1000 \text{ V cm}^{-1}$  for MgO-doped alumina. However, this temperature was determined at the very late stage of the shrinkage; extrapolation to the earlier stages of densification is in agreement with the

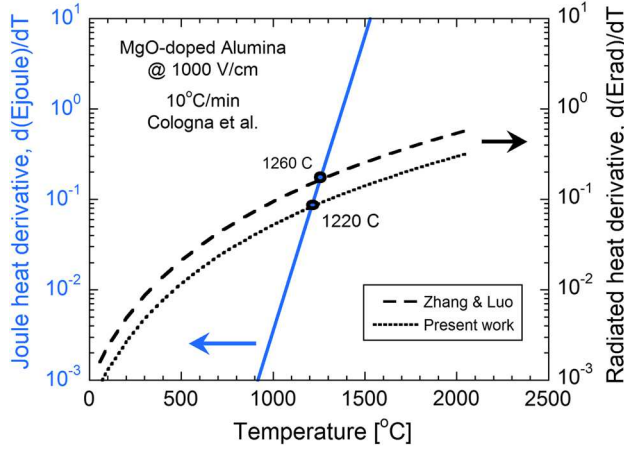


**Figure 1** Joule heat and radiated heat derivatives versus temperature. The flash temperature is determined at the intersection when the rate of the generated Joule heat surpasses the rate of the dissipated heat by radiation. Flash temperatures of 1220 and 1260 °C were determined, respectively, assuming partial (dotted curve) and total loss (dashed curve) of the generated Joule heat by radiation from the specimen's surfaces.

lower flash temperature of 1220 °C, as is in our calculation.

Second, let us assume heating the specimen from room temperature to above its melting point, without an electric field. It will generate internal heat corresponding to the heat capacity of the specimen mass, as a solid and as a liquid. The internal heats [Eq. (9)] that the alumina specimen [2] can store as a solid bulk, as a partially melted solid (at the percolation threshold), and as fully liquid, were calculated versus temperature, and shown in Fig. 2. The internal heat in the solid state (solid red curve in Fig. 2) increases with temperature up to the melting point ( $T_m = 2050$  °C). At this temperature, melting is associated with an enthalpy of fusion, due to the endothermic nature of the melting. The internal heat of the fully melted specimen (dotted black line) is also shown in Fig. 2. The internal heat of the partially melted solid at the percolation threshold, i.e., solid with liquid volume fraction of 0.247 (formed only at the previously calculated flash temperature) also is shown in Fig. 2 (dashed-dotted blue curve). We calculated the internal heat for this percolating system using the phase assemblage Eq. (10) in the “Appendix” section. The hatched area in Fig. 2 represents the excess internal heat between the percolating system and its non-percolating solid counterpart. This excess heat represents the heat invested for partial

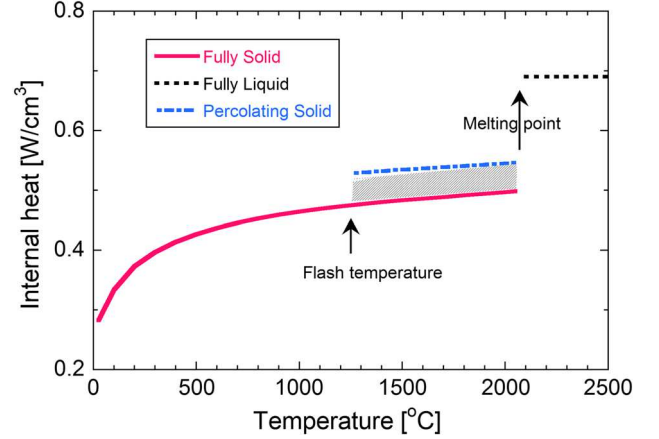


**Figure 2** Internal heat versus temperature in MgO-doped alumina specimen similar to that in Ref. [2] assuming fully solid granular (solid red curve), granular solid with percolation through the liquid (dashed-dotted blue curve), and fully liquid (dotted black line). The hatched area represents the excess internal heat needed to form the percolating liquid at the flash temperature.

melting as needed in the percolative system. For the sake of simplicity, we assumed constant volume fraction of the liquid at the percolation threshold up to the melting temperature. Nevertheless, we do not know how and whether the liquid fraction changes (increases) with the temperature increase. Since local melting is associated with decrease in the local electric resistivity, the melted contact loci is no more a preferred site for local Joule heating. Consequently, it will solidify after local particle rearrangement hence decrease the melt volume fraction. Such self-regulating nature of the powder compact with respect to formation of local liquid and its solidification is in accord with our assumption on constant volume fraction of the melt. Below we will compare this excess internal heat to the excess Joule heat absorbed by the internal particles versus temperature. The temperature at which the excess Joule heat surpasses the excess internal heat of the percolating system determines the surface temperature of the internal particles, at which local melting can take place at their contact points.

Third and last, we calculated the excess Joule heat of the specimen with the simultaneous radiation loss. The excess Joule heat is the difference between the generated Joule heat and the heat radiated from the specimen surfaces in Eq. (6). Although the furnace temperature is constant during the real experiment, the internal temperature of the specimen increases with time, due to Joule heating. Thus, calculation of



various heats versus temperature is justified, since the flash sintering experiment does not end with the flash event. The specimen is continuously heated by the Joule heating until the constant current limitation is activated. During this period (stage II in flash sintering), between the flash event and the constant current, the temperature of the internal particles may increase. We calculated the excess Joule heat versus temperature and compared it with the excess internal heat due to the partial melting (percolating solid), as shown in Fig. 3. As mentioned above, partial melting may take place at the temperature, when the gain in the excess Joule heat surpasses the heat invested for the partial melting. For comparison, the heat needed for full melting of the specimen also is shown in Fig. 3 (horizontal dotted blue line). It is clear from Fig. 3, that already at the flash temperature (regardless whether 1220 or 1260 °C), the excess Joule heat is higher by one to two orders of magnitude than those needed for partial or full melting of the specimen.

## Discussion

Our calculations above highlighted a few new heat aspects during the flash sintering, using MgO-doped alumina as a reference. First, the assumption that heat is lost by radiation only from the nanoparticles at the external surfaces did not change significantly the calculated onset temperature for the flash event. We calculated the temperature of 1220 °C, compared to

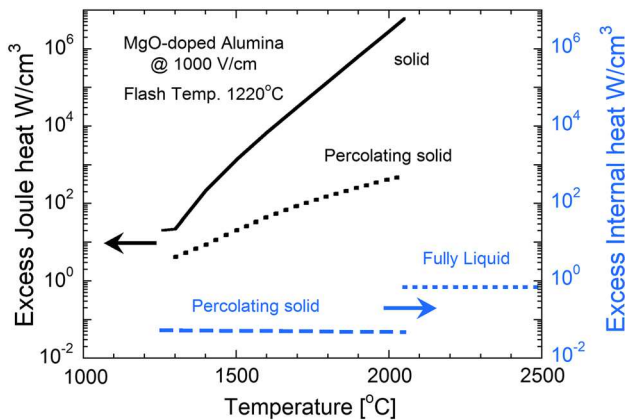


**Figure 3** Excess Joule heat generated, and excess internal heat needed to form a liquid, versus temperature, for MgO-doped alumina specimen in Ref. [2] at different states. The states include fully solid granular, fully liquid, and granular solid with percolation through the liquid.

the reported temperature of 1260 °C [2]. Careful observation of the shrinkage curve in dilatometer (i.e., Figure 4b in Ref. [2]) reveals its gradual increase with the temperature increase. The higher temperature of 1260 °C was determined at a relatively advanced stage of the shrinkage [2]. Therefore, a temperature interval exists over which the flash can be detected, and the flash temperature of 1220 °C can easily be included in that interval. Although these temperatures may be important, they do not provide information about the active densification mechanisms after the flash event.

The evolution of the internal heat with temperature in the specimen (Fig. 2) reveals the amount of the extra heat needed to initiate local surface softening/melting (hatched area in Fig. 2). This excess heat increases the solid internal heat only by 10%, but may have significant effect on the sintering kinetics. Melting is an endothermic reaction, therefore local melting is associated with activation energy to initiate the melt from the crystal. In this respect, application of external fields on crystals and glasses (even with no contact electrodes) was found to enhance reorientation of the surface dipoles [48], increase the structural disorder at the surface [49], and enhance the softening of glasses [4]. The electric field-induced softening (EFIS) of the glass was related to combination of Joule heating, dielectric breakdown, and electrolysis within the glass. The application of external electric field combined with thermal heat expected to increase the entropy, hence induce amorphicity [47]. Flash experiments of porcelain by Biesuz et al. [50] together with fast heating without an electric current confirmed the direct effect of the electric field on softening of the glassy phase at lower temperatures. The effect of rapid sintering due to rapid heating in the absence of electric field [22] was marginal in amorphous porcelain [50].

The effect of non-contacting electric field on rapid densification of partially stabilized zirconia [51] and ( $K_{0.5}Na_{0.5}$ )  $NbO_3$  [36] showed clear evidence for liquid in the latter. Muccillo et al. [46] reported on melting of the 8YSZ specimens subjected to flash sintering when the current surpassed a critical value. These findings reveal that the charged nature of the ceramic nanoparticle surfaces and their nano-size are the main cause for the electric field effects. Once the nanoparticles rearranged and densified by the local melt, due to the induced attractive capillary forces, the liquid solidifies to lower the internal heat.

Therefore, the decrease in the internal heat, which is associated with the solidification of the melt, is compatible with the transient nature of the melt that forms at the nanoparticle contacts. The thickness of the softened/melted surface of a few atomic layers suffices for the nanoparticle reorientation as needed for the local densification. The nanograin clusters found in many flash sintered systems may be the manifestation of these reorientations [52]. These effects may explain the lack of remnant liquid in flash sintered nanoparticles.

Comparison between the excess Joule heat and the excess internal heat needed for percolative local melting (Fig. 3) reveals the far higher values of the former. It turns out that the excess Joule heat generated already at the flash event suffices to induce local melting at the nanoparticle contacts. It also suffices to induce full melting in the specimen. A similar trend exists assuming a fully solid granular compact.

Flash sintering and spark plasma sintering, albeit activated at different temperature-electric field conditions, represent the two edges of a same process. Simulation of the spark plasma sintering process of Si nanoparticles, assuming current percolation, was consistent with full melting and recrystallization of the specimen [53]. Local melting on the surfaces of cuboidal-shape LiF microcrystals was clearly observed during the spark plasma sintering as shown in Fig. 4 [54]. Several reasons can be accounted for why such a catastrophic melting was not observed in flash sintered specimens. First, the flash experiments are controlled by limiting the current density

immediate to the flash event. If this limitation is removed, the excess Joule heat may locally melt the compact [35], or fully melt the glass (see supplement in Ref. [4]). Second, as shown and argued above, the liquid has a transient nature. Once it aided to rearrange locally the nanoparticles, the contact points are lost, and the local electric resistance decreases, compared to neighbor sites where non-dense nanoparticles with high contact resistance exist. As a result, the local melt will solidify, which is in agreement with the trend for energy minimization in the system. Our present treatment reveals the nature of the so-called thermal runaway during the flash sintering as local melting followed by local exothermic solidification.

Another consequence from the present calculations is that the surface temperature of the internal particles,  $T_p$ , does not need to be far higher than that of the particles at the specimen's surface,  $T_{surf}$ , for inducing the local softening/melting. Accounting for the actual physics of the process, the calculated excess Joule heat can be distributed in the non-homogeneous manner within the specimen, i.e., along the percolative backbone. This will enhance the intensity of the Joule heat, with consequent local macroscopic melting. Therefore, current control in stage II of flash sintering is targeted toward a more homogeneous heating of the specimen. Very recently, Yadav and Raj [55] showed that Debye temperature is the lower limit for the flash onset temperature; they related the flash event at the first stage of flash sintering to nonlinear thermal vibrations, which is in accord with our local melting at the nanoparticle surfaces.

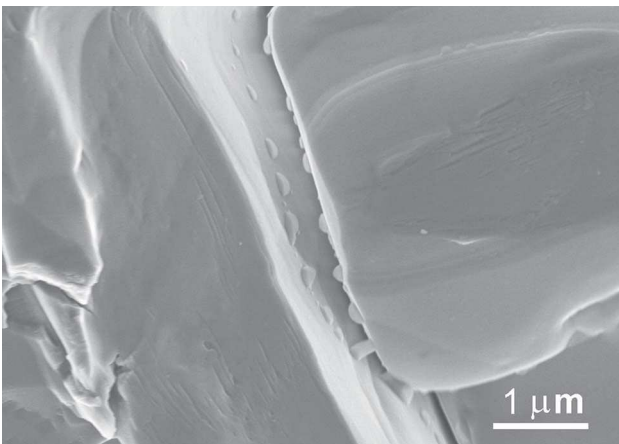


**Figure 4** Local melting observed during interrupted spark plasma sintering experiments using LiF microcrystals heated to 500 °C under 2 MPa applied pressure [54].

## Summary and conclusions

The surface softening/melting model for flash sintering of oxide nanoparticles considered the heat balance at the flash event. The higher electric resistance at the nanoparticle contact points leads to preferred Joule heating at these loci. At first, the generated heat is dissipated within the adjacent nanoparticles and increases their temperature. Analysis of the heat transfer indicates negligible heat loss by convection/conduction from the heated nanoparticles. The main heat loss is by radiation from the nanoparticles at the external surfaces of the specimen, where the nanoparticles within the specimen volume inter-radiate to each other, hence their heat is preserved. The Knudsen layer formed at the

nanoparticle surface can establish surface temperatures and temperature gradients as high as twice the gas's temperature that surrounds the internal nanoparticles. Consequently, very high temperatures may develop at the nanoparticle surfaces. The excess Joule heat at the flash temperature suffices the excess heat necessary for local contact softening/melting, through which the electric current percolates. Formation of liquid at the contact points increases the overall electric conductivity by two to four orders of magnitudes and enables the rapid densification kinetics by nanoparticle rearrangement and densification aided by the attractive capillary forces of the melt. The transient nature of the local melt leads to its solidification immediate to the nanoparticle rearrangement. Therefore, thermal runaway in flash sintering refers to the local softening/melting at the nanoparticle surfaces and their immediate solidification.

## Acknowledgements

R. Chaim acknowledges the warm and kind hospitality of the colleagues from CIRIMAT during his sabbatical stay in Toulouse, where this paper was prepared. We thank Dr. Rachel Marder for kindly providing the Fig. 4.

## Compliance with ethical standards

**Conflict of interest** All authors declare that they have no conflict of interest.

## Appendix Thermal heat

The internal heat was calculated using the following equation:

$$\dot{Q}_{\text{int}} = \rho_g \rho_0(T) c_p(T) \frac{dT}{dt} \quad (9)$$

While neglecting the change in the green density up to the flash temperature, which fairly is correct [56]. The temperature-dependent specific heat of solid alumina was used, up to its melting point.

When liquid forms, most probably at the nanoparticle contacts, the change in the internal heat was calculated according to the following equation [47]:

$$\dot{Q}_{\text{int}} = \left[ \rho_s c_p^{\text{solid}} (1 - x_{\text{melt}}) + \rho_l c_p^{\text{liquid}} x_{\text{melt}} \right] \frac{dT}{dt} \quad (10)$$

where  $x_{\text{melt}}$  is the volume fraction of the melt, and indices s and l refer to solid and liquid, respectively. Since current percolation is associated with the percolation phenomenon, the volume fraction of the melt is 0.247 at the invasive percolation threshold [57]. This value was used to calculate the heat capacity of the specimen when liquid forms.

For heat/energy balance, we added the enthalpy of fusion at the percolation threshold (i.e., for fusion of 0.247 volume fraction of the mass) to the internal heat versus temperature (see the shaded area in Fig. 2).

The internal heat in Eq. (9) was calculated using the finite differences approximation described elsewhere [18]:

$$\dot{Q}_{\text{int}} = \rho_g \rho_0(T_i) c_p(T_i) \frac{T_p^{i+1} - T_p^i}{\Delta t} \quad (11)$$

where the interval between two consecutive temperatures and their corresponding time interval  $\Delta t$  were determined from the heating rate during the experiment [2].

The following temperature-dependent functions were used:

- (a) Temperature dependencies of the density ( $\text{g cm}^{-3}$ ) of solid  $\text{Al}_2\text{O}_3$  and its melt (liquid) [58]:

$$\rho_s = 3.9899 - 12 \times 10^{-5} \cdot T(^{\circ}\text{C}) \quad (12)$$

$$\rho_l = 5.3243 - 11.27 \times 10^{-4} \cdot T(^{\circ}\text{C}) \quad (13)$$

- (b) Temperature dependence of the specific heat of solid and liquid  $\text{Al}_2\text{O}_3$  ( $\text{J mol}^{-1} \text{K}^{-1}$ ) [59]:

$$c_p^{\text{solid}} = 102.43 + 38.75 \cdot \theta - 15.91 \cdot \theta^2 + 2.63 \cdot \theta^3 - \frac{3.0075}{\theta^2} \quad (14)$$

in the temperature range 298–2327 K

$$c_p^{\text{liquid}} = 192.46 + 9.52 \times 10^{-8} \cdot \theta - 2.85 \times 10^{-8} \cdot \theta^2 + 2.93 \times 10^{-9} \cdot \theta^3 - \frac{5.59 \times 10^{-8}}{\theta^2} \quad (15)$$

in the temperature range 2327–4000 K

$$\text{Where } \theta = \frac{T(\text{K})}{1000}$$

## Joule heat

The accumulated Joule heat was calculated using the following equation:

$$\dot{Q}_{\text{Joul}} = \int_{t=0}^{t(T_{\text{onset}})} \frac{V^2}{R_e(T)} dt \quad (16)$$

The temperature dependence of the electric resistivity of pure  $\text{Al}_2\text{O}_3$  is strongly affected by the impurity content. Therefore, published data about flash sintering of alumina was used together with the specimen dimensions and the flash process parameters [2]. The average electric conductivity of the present alumina is therefore:

$$\sigma_{\text{Solid}}^{\text{Alumina}} = 3.289(\Omega \text{ cm})^{-1} \cdot e^{-\left[\frac{21253}{T(\text{K})}\right]} \quad (17)$$

and the electric conductivity of alumina melt is [25]:

$$\sigma_{\text{melt}}^{\text{Alumina}} = 0.0032213(\Omega \text{ cm})^{-1} \cdot e^{-[0.0019314 \cdot T(\text{K})]} \quad (18)$$

The Joule heat prior to any melt was calculated using the solid phase properties, both as dense, as well as a granular (percolative) system [34]. However, at the current percolation threshold, when continuous liquid forms, the specimen properties of a percolating media (with liquid volume fraction of 0.247) were used [34]:

$$\sigma_{\text{specimen}}^{\text{percol}} = (\sigma_{\text{solid}})^{0.72} \cdot (\sigma_{\text{melt}})^{0.28} \quad (19)$$

## References

- [1] Cologna M, Rashkova B, Raj R (2010) Flash sintering of nanograin zirconia in < 5 s at 850 C. *J Am Ceram Soc* 93:3556–3559
- [2] Cologna M, Francis JSC, Raj R (2011) Field assisted and flash sintering of alumina and its relationship to conductivity and MgO-doping. *J Eur Ceram Soc* 31:2827–2837
- [3] Lebrun JM, Raj R (2014) A first report of photoemission in experiments related to flash sintering. *J Am Ceram Soc* 97:2427–2430
- [4] McLaren C, Heffner W, Tassarollo R, Raj R, Jain H (2015) Electric field-induced softening of alkali silicate glasses. *A Phys Lett* 107:184101. Supplementary material at <http://dx.doi.org/10.1063/1.4934945>
- [5] Naik K, Jha SK, Raj R (2016) Correlation between conductivity, electroluminescence and flash sintering. *Scr Mater* 118:1–4
- [6] McLaren C, Roling B, Raj R, Jain H (2017) Mechanism of electric field-induced softening (EFIS) of alkali silicate glasses. *J Non Cryst Solids* 471:384–395
- [7] Biesuz M, Luchi P, Quaranta A, Martucci A, Sglavo VM (2017) Photoemission during flash sintering: an interpretation based on thermal radiation. *J Eur Ceram Soc* 37:3125–3130
- [8] Downs JA, Sglavo VM (2013) Electric field assisted sintering of cubic zirconia at 390 C. *J Am Ceram Soc* 96:1342–1344
- [9] Dong Y, Chen IW (2015) Predicting the onset of flash sintering. *J Am Ceram Soc* 98:2333–2335
- [10] Biesuz M, Luchi P, Quaranta A, Sglavo VM (2016) Theoretical and phenomenological analogies between flash sintering and dielectric breakdown in  $\alpha$ -alumina. *J Appl Phys* 120:145107
- [11] Du Y, Stevenson AJ, Vernat D, Diaz M, Marinha D (2016) Estimating Joule heating and ionic conductivity during flash sintering of 8YSZ. *J Eur Ceram Soc* 36:749–759
- [12] Raj R (2016) Analysis of the power density at the onset of flash sintering. *J Am Ceram Soc* 99:3226–3232
- [13] Chaim R (2017) Particle surface softening as universal behaviour during flash sintering of oxide nano-powders. *Materials* 10:179
- [14] Todd RI, Zapata-Solvas E, Bonilla RS, Sneddon T, Wilshaw PR (2015) Electrical characteristics of flash sintering: thermal runaway of Joule heating. *J Eur Ceram Soc* 35:1865–1877
- [15] Zhang Y, Jung J, Luo J (2015) Thermal runaway, flash sintering and asymmetrical microstructural development of ZnO and ZnO– $\text{Bi}_2\text{O}_3$  under direct currents. *Acta Mater* 94:87–100
- [16] Pereira da Silva JG, Al-Qureshi HA, Keil F, Janssen R (2016) A dynamic bifurcation criterion for thermal runaway during the flash sintering of ceramics. *J Eur Ceram Soc* 36:1261–1267
- [17] Biesuz M, Sglavo VM (2016) Flash sintering of alumina: effect of different operating conditions on densification. *J Eur Ceram Soc* 36:2535–2542
- [18] Shomrat N, Baltianski S, Dor E, Tsur Y (2017) The influence of doping on flash sintering conditions in  $\text{SrTi}_{1-x}\text{Fe}_x\text{O}_{3-\delta}$ . *J Eur Ceram Soc* 37:179–188
- [19] Jiang T, Wang Z, Zhang J, Hao X, Rooney D, Liu Y, Sun W, Qiao J, Sun K (2015) Understanding the flash sintering of rare-earth-doped Ceria for solid oxide fuel cell. *J Am Ceram Soc* 98:1717–1723
- [20] Muccillo R, Kleitz M, Muccillo ENS (2011) Flash grain welding in yttria-stabilized zirconia. *J Eur Ceram Soc* 31:1517–1521

- [21] Raj R (2012) Joule heating during flash-sintering. *J Eur Ceram Soc* 32:2293–2301
- [22] Ji W, Parker B, Falco S, Zhang JY, Fu ZY, Todd RI (2017) Ultra-fast firing: effect of heating rate on sintering of 3YSZ, with and without an electric field. *J Eur Ceram Soc* 37:2547–2551
- [23] Bykov YV, Egorov SV, Ereemeev AG, Kholoptsev VV, Rybakov KI, Sorokin AA (2015) Flash microwave sintering transparent Yb (LaY)<sub>2</sub>O<sub>3</sub> ceramics. *J Am Ceram Soc* 98:3518–3524
- [24] Narayan J (2013) Grain growth model for electric-assisted processing and flash sintering of materials. *Scr Mater* 68:785–788
- [25] Chaim R (2016) Liquid film capillary mechanism for densification of ceramic powders during flash sintering. *Materials* 9:280
- [26] Corapcioglu G, Gulgun MA, Kisslinger K, Sturm S, Jha SK, Raj R (2016) Microstructural and microchemistry of flash sintered K<sub>0.5</sub>Na<sub>0.5</sub>NbO<sub>3</sub>. *J Ceram Soc Japan* 124:321–328
- [27] Grasso S, Sakka Y, Rendtorff N, Hu C, Maizza G, Borodianska H, Vasylykiv O (2011) Modeling of the temperature distribution of flash sintered zirconia. *J Ceram Soc Japan* 119:144–146
- [28] Terauds K, Lebrun JM, Lee HH, Jeon TY, Lee SH, Je JH, Raj R (2015) Electroluminescence and the measurement of temperature during stage III of flash sintering experiments. *J Eur Ceram Soc* 35:3195–3199
- [29] Park J, Chen IW (2013) In situ thermometry measuring temperature flashes exceeding 1700 C in 8 mol% Y<sub>2</sub>O<sub>3</sub>-stabilized zirconia under constant-voltage heating. *J Am Ceram Soc* 96:697–700
- [30] Lebrun JM, Jha SK, McCormack SJ, Kriven WM, Raj R (2016) Broadening of diffraction peak widths and temperature nonuniformity during flash experiments. *J Am Ceram Soc* 99:3429–3434
- [31] Pereira da Silva JG, Lebrun JM, Al-Qureshi HA, Janssen R, Raj R (2015) Temperature distribution during flash sintering of 8% yttria-stabilized zirconia. *J Am Ceram Soc* 98:3525–3528
- [32] Dong Y, Chen IW (2016) Thermal runaway in mold-assisted flash sintering. *J Am Ceram Soc* 99:2889–2894
- [33] Holland TB, Anselmi-Tamburini U, Quach DV, Tran TB, Mukherjee AK (2012) Effects of local Joule heating during the field assisted sintering of ionic ceramics. *J Eur Ceram Soc* 32:3667–3674
- [34] Chaim R, Weibel A, Chevallier G, Estournès C (2017) Flash sintering of dielectric nanoparticles as a percolation phenomenon through a softened film. *J Appl Phys* 121:145103
- [35] Yoshida H, Uehashi A, Tokunaga T, Sasaki K, Yamamoto T (2016) Formation of grain boundary second phase in BaTiO<sub>3</sub> polycrystal under a high DC electric field at elevated temperatures. *J Ceram Soc Jpn* 124:388–392
- [36] Chen K, Jiao Y, Zhao Y, Gao Y, Zhang X, An L (2017) Non-contact electric field-enhanced abnormal grain growth in (K<sub>0.5</sub>Na<sub>0.5</sub>) NbO<sub>3</sub> ceramics. *Ceram Int* 43:12343–12347
- [37] Du B, Gucci F, Porwal H, Grasso S, Mahajan A, Reece MJ (2017) Flash spark plasma sintering of magnesium silicide stannide with improved thermoelectric properties. *J Mater Chem C* 5:1514–1521
- [38] Kocjan A, Logar M, Shen Z (2017) The agglomeration, coalescence and sliding of nanoparticles, leading to the rapid sintering of zirconia nanoceramics. *Sci Rep* 7:2541
- [39] Liu F, Daun KJ, Snelling DR, Smallwood GJ (2006) Heat conduction from a spherical nano-particle: status of modeling heat conduction in laser-induced incandescence. *Appl Phys B* 83:355–382
- [40] Yoshida H, Morita K, Kim BN, Sakka Y, Yamamoto T (2016) Reduction in sintering temperature for flash-sintering of yttria by nickel cation-doping. *Acta Mater* 106:344–352
- [41] Merabia S, Shenogin S, Joly L, Keblinski P, Barrat JL (2009) Heat transfer from nanoparticles: a corresponding state analysis. *PNAS* 106:15113–15118
- [42] Merabia S, Keblinski P, Joly L, Lewis LJ, Barrat JL (2009) Critical heat flux around strongly heated nanoparticles. *Phys Rev E* 79:021404
- [43] Zhang Y, Luo J (2015) Promoting the flash sintering of ZnO in reduced atmospheres to achieve nearly full densities at furnace temperatures < 120 C. *Scr Mater* 106:26–29
- [44] Olevsky EA, Rolfing SM, Maximenko AL (2016) Flash (ultra-rapid) spark-plasma sintering of silicon carbide. *Sci Rep* 6:33408
- [45] Smith WF, Hashemi J (2000) Foundations of materials science and engineering. McGraw Hill, Boston, p 616
- [46] Muccillo R, Muccillo ENS (2013) An experimental setup for shrinkage evaluation during electric field-assisted flash sintering: application to yttria-stabilized zirconia. *J Eur Ceram Soc* 33:515–520
- [47] Michelsen HA (2003) Understanding and predicting the thermal response of laser-induced incandescence from carbonaceous particles. *J Chem Phys* 118:7012–7045
- [48] Fu H, Cohen RE (2000) Polarization rotation mechanism for ultrahigh electromechanical response in single-crystal piezoelectrics. *Nature* 403:281–283
- [49] Johari GP (2013) Effects of electric field on the entropy, viscosity, relaxation time, and glass-formation. *J Chem Phys* 138:154503
- [50] Biesuz M, Abate WD, Sglavo VM (2017) Porcelain stoneware consolidation by flash sintering. *J Am Ceram Soc* 101:71–81

- [51] Majidi H, van Benthem K (2015) Consolidation of partially stabilized  $\text{ZrO}_2$  in the presence of a noncontacting electric field. *Phys Rev Lett* 114:195503
- [52] Chaim R, Chevallier G, Weibel A, Estournès C (2018) Grain growth during spark plasma and flash sintering of ceramic nanoparticles: a review. *J Mater Sci* 53:3087–3105. <https://doi.org/10.1007/s10853-017-1761-7>
- [53] Schwesig D, Schierner G, Theissmann R, Stein N, Petermann N, Wiggers H, Schmechel R, Wolf DE (2011) From nanoparticles to nanocrystalline bulk: percolation effects in field assisted sintering of silicon nanoparticles. *Nanotechnology* 22:135601
- [54] Marder R, Estournès C, Chevallier G, Chaim R (2014) Plasma in spark plasma sintering of ceramic particle compacts. *Scr Mater* 82:57–60
- [55] Yadav D, Raj R (2017) Two unique measurements related to flash experiments with yttria-stabilized zirconia. *J Am Ceram Soc* 100:5374–5378
- [56] Karakuscu A, Cologna M, Yarotski D, Won J, Francis JSC, Raj R, Uberuaga BP (2012) Defect structure of flash-sintered strontium titanate. *J Am Ceram Soc* 95:2531–2536
- [57] Gouyet JF (1996) *Physics and fractal structures*. Masson, New York
- [58] Kirshenbaum AD, Cahill JA (1960) The density of liquid aluminium oxide. *J Inorg Nucl Chem* 14:283–287
- [59] Chase MW (1998) NIST-JANAF thermochemical tables. *J Phys Chem Ref Data Monogr* 9:1–1951